PROC. OF JSCE,
No. 286, JUNE 1979

EXPERIMENTAL STUDY ON THE ULTIMATE STRENGTH OF STEEL ARCHES

By Tatsuro SAKIMOTO, Toshitaka YAMAO** and Sadao KOMATSU****

1. INTRODUCTION

Since the recent trend of development in steel bridges is toward more long-spanned structures in use of high-strength steel and the advanced welding technology, the lateral stability of the bridge in the elasto-plastic range poses various important problems.

Many studies have been reported in reference to the elastic lateral stability of arches[1),2)], but few have been made on the inelastic lateral stability of arches[3)~6)]. It has been in recent years that experimental studies on the inelastic lateral strength of arches were taken up as the subject of some investigators.[7)]

The purpose of this experimental investigation is to present fundamental data concerning the inelastic lateral strength of steel arches. To examine the validity of the theoretical result presented previously by the writers[8)] is also one of main aims of this study.

It is well known that the ultimate strength and the elasto-plastic behavior of compressive members are much affected by unavoidable imperfections such as the residual stress due to welding and initial lateral crookedness[9)]. This fact seems to be true also in steel arches theoretically[4),6)]. Furthermore, it is very possible that the wind load or the earthquake load is the governing design load and they may cause the collapse of bridge arches. Accordingly, ordinary bridge arches are composed of twin ribs braced with lateral members of truss or transverse beams of Vierendeel type to increase the lateral stability. The type and the stiffness of lateral bracing members may be very important factors controlling the lateral strength of bridge arches directly[10)~13)].

Considering above-mentioned circumstances, the model tests are conducted with special attention to the following items; (1) influence of residual stresses and initial lateral crookedness, (2) influence of the arch configuration (circular and parabolic), (3) effects of the type, the location and the stiffness of the bracing member, (4) comparison of the ultimate strength between the single arch and the twin arches with lateral bracing members, and (5) ultimate strength of arches subjected to both in-plane vertical load and lateral horizontal load.

2. EXPERIMENTAL PROGRAM

(1) Design Concept of the Model Arch

Nominal dimensions of the model arch are determined according to the following conditions:

1) The model arch is a circular or a parabolic one of through type with two-hinged end condition, and its non-dimensional parameters have almost the same order as those of existing actual bridges. All the displacement and rotation are restrained at both ends of arch ribs except the in-plane rotation about the horizontal axis.
2) The slenderness ratio of the arch rib is determined so that the arch fails owing to an overall instability in the elasto-plastic range.
3) The cross section of the arch rib is a welded single-cell box and its size is large enough to measure accurately the residual stress distribution.
4) The component plates of the box section should not fail owing to a local buckling previously to the overall instability of the arch.
5) The vertical maximum load must be less than the maximum capacity of an available hydraulic jack, which is 30 tons by itself and

* Ms. of Eng., Asst. Prof. of Civil Eng., Kumamoto Univ.
** Ms. of Eng., Research Asisstant of Civil Eng., Kumamoto Univ.
*** Dr. of Eng., Prof. of Civil Eng., Osaka Univ.

Table 1 Nominal Dimensions of the Model Arch.

Test of Series	l mm	L mm	f mm	f/l	t mm	e mm	h mm	A cm^2	I_x cm^4	I_y cm^4	I_z cm^4	$\frac{GI_x}{EI_y}$	r_y mm	L/r_y
Circular	2800	3110	560	0.2	4.5	4.5	59	9.00	42.4	32.7	34.6	0.52	19.6	159
Parabolic	2800	3070	560	0.2	4.5	2.5	55	8.64	42.4	30.9	31.6	0.50	19.1	161
Remarks	See Fig. 1 Cross-sectional properties are about one arch rib A =cross-sectional area I_x, I_y, I_z=moment of inertia of the cross section with respect to x, y and z-axes, respectively r_y =radius of gyration of the cross section													

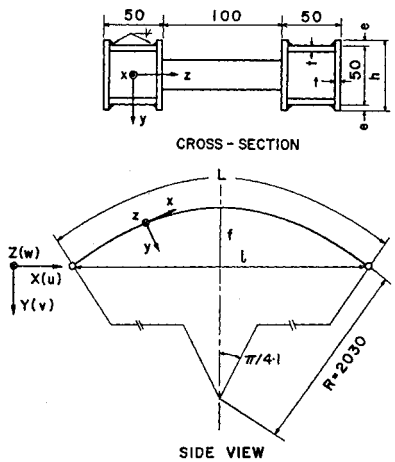

Fig. 1 Configuration of the Model Arch (unit in mm).

60 tons by using a lever beam.

The nominal dimensions of the model arch are shown in Table 1 and Fig. 1, where the radius R and the central angle of the arch are defined only for the circular arch.

(2) Lateral Bracing Members

The lateral deformation of the arch is characterized by the interaction between the lateral deflection and the torsional deformation. So, three types of the bracing member shown in Fig. 2 are designed to resist these deformations, correspondingly. The first type, type P, mainly resists torsion of the arch ribs. The second one, type L, mainly resists the lateral bending of the arch ribs. These two types of transverse beams and the magnitude of their bending stiffness are determined to simulate the Vierendeel beam used in actual arch bridges. The third one, type X, is a truss of double Warren type, which works like the beam of type L. To avoid the premature buckling of the bracing member, the slenderness ratio of the truss member is determined to

Table 2 Dimensions and Properties of Bracing Members.

Beams	a(cm)×b(cm)	I_b(cm^4)	I_y(cm^4)	$I_b/I_y\times100$(%)
B_1	3.0×1.0	2.25	32.7	6.9
B_2	3.7×0.9	3.80	30.9	12.3
B_3	5.5×0.9	12.5	30.9	40.4
Truss	d (cm)	A_t(cm^2)	r_t (cm)	$\lambda_t=l_t/r_t$
T_1	0.9	0.64	0.23	50
T_2	1.6	2.01	0.40	28
Remarks	See Fig. 2 I_b=moment of inertia of transeverse beam section with respect to the strong axis l_t=effective buckling length of the truss members r_t=radius of gyration of the truss members A_t=cross-sectional area of the truss members			

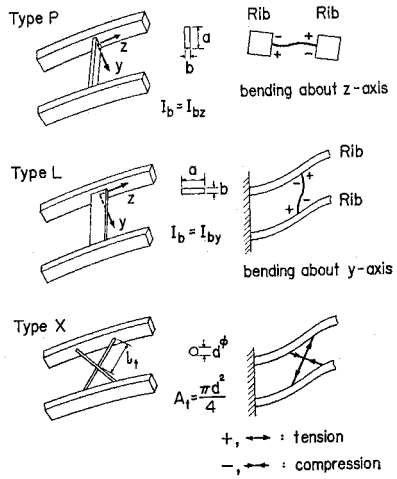

Fig. 2 Arrangement and Induced Deformations of Bracing Members.

be much smaller than that of ordinary actual bridge, which is determined to resist mainly the wind force or the earthquake force. The bracing member of double Warren type is welded to the

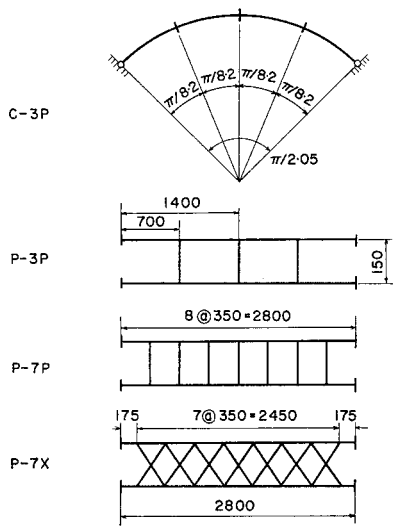

Fig. 3 Bracing Systems (unit in mm).

arch ribs at the nodal point. The dimensions and properties of bracing members are shown in Table 2 and the induced deformation patterns are illustrated in Fig. 2. The number and the arranging manner of the bracing members are shown in Fig. 3.

(3) Load Conditions and Notation of the Model

Main load conditions adopted in the test are the uniformly distributed vertical load and a combination of uniform vertical load and

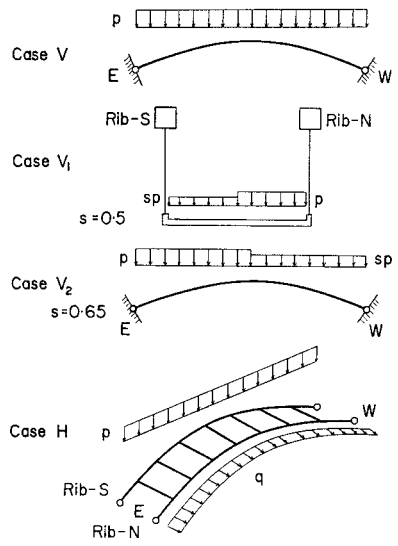

Fig. 4 Load Conditions.

Table 3 List of Test Specimens.

No.	Name of Specimens	Configuration	Bracings			Loading	
			Number	Type	Dimension	Direction	Conditions
1	C-S-V	Circular	S			V.D.	Uniform
2	C-3P-V	Circular	3	V	B_1	V.D.	Uniform
3	C-3L-V	Circular	3	V	B_1	V.D.	Uniform
4	P-S-V	Parabolic	S			V.D.	Uniform
5	P-3P-V	Parabolic	3	V	B_2	V.D.	Uniform
6	P-3L-V	Parabolic	3	V	B_2	V.D.	Uniform
7	P-7P-V_1	Parabolic	7	V	B_2	V.D.	Transversely nonuniform
8	P-7X-V_1	Parabolic	7	T	T_1	V.D.	Transversely nonuniform
9	P-S-V_2	Parabolic	S			V.D.	Longitudinaly nonuniform
10	P-7P-H	Parabolic	7	V	B_3	H.D.	with Uniform Vertical Load
11	P-7L-H	Parabolic	7	V	B_3	H.D.	with Uniform Vertical Load
12	P-7X-H	Parabolic	7	T	T_2	H.D.	with Uniform Vertical Load
Remarks	S=Single Arch V=Vierendeel T=Truss					V.D.=Vertical Direction H.D.=Horizontal Direction	

horizontal one. Unsymmetrical loading cases both in transverse and longitudinal directions shown in Fig. 4 are also studied for some specimens. The names of the specimens are summarized in Table 3. The letters in the notations, C–3P–V, P–7X–H, etc., refer to the configuration, the number and the type of the bracing member, as well as the load condition, in this order. The both springings of arch ribs denoted by the letters E and W, and the individual arch rib is distinguished as rib-S or rib-N from each other.

(4) Preliminary Tests

The average values of standard tensile coupon tests are shown in Table 4 with those of mill sheets. The value of the yield strain ϵ_y is determined as the strain at which an appreciable plastic flow initiates. The measured value is used thereafter for evaluating the test data.

The box section of the arch rib is built up by manual welding. The running velocity of the welding electrode is about 50 cm/min. under the electric conditions of 30 Volts and 130 Amperes. The measurement of the residual stress is performed by a sectioning method using a strain measuring device of Hüggenberger type. The measured values are modified so as to satisfy the self-equilibrium conditions as well as doubly symmetric conditions. The modified distribution of residual stress is shown in Fig. 5 together

Table 4 Mechanical Properties of the Materials.

Properties \ Test Series	Circular		Parabolic	
	Mill Sheet	Measured Values	Mill Sheet	Measured Values
Plate Thickness t mm	4.5	5.1	4.5	4.6
Young's Modulus E kg/cm²	—	1.98×10^6	—	2.18×10^6
Yield Stress σ_y kg/cm²	2 900	3 180	3 600	3 640
Max. Strength σ_m kg/cm²	4 300	4 427	4 800	4 498
Yield Strain $\varepsilon_y\times10^{-6}$	—	2 000	—	2 000
Elongation e %	40.0	36.7	34.0	32.1

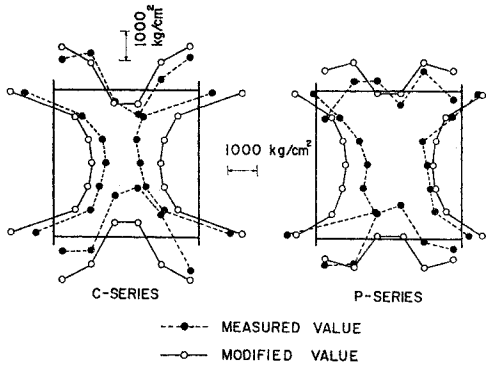

Fig. 5 Residual Stress Distributions.

Table 5 Initial Lateral Crookedness.

Test Specimens	Max. Values	Modes
1 (C-S-V)	l/1480	W — E
2 (C-3P-V)	Rib-N l/1230 l Rib-S l/1480 l	
3 (C-3L-V)	Rib-N l/550 l Rib-S l/940 l	
4 (P-S-V)	l/1140 l	
5 (P-3P-V)	Rib-N l/690 l Rib-S l/760 l	
6 (P-3L-V)	Rib-N l/1120 l Rib-S l/1520 l	
7 (P-7P-V_1)	Rib-N l/1010 l Rib-S l/1320 l	
8 (P-7X-V_1)	Rib-N l/190 l Rib-S l/300 l	
9 (P-S-V_2)	l/1270 l	
10 (P-7P-H)	Rib-N l/1640 l Rib-S l/660 l	
11 (P-7L-H)	Rib-N l/740 l Rib-S l/550 l	
12 (P-7X-H)	Rib-N l/270 l Rib-S l/620 l	

with the measured value. Thus the maximum compressive residual stress is estimated at 0.41 σ_y for web plates and 0.15 σ_y for flange plates in Circular series, and in Parabolic series, at 0.27 σ_y for web plates and 0.01 σ_y for flange plates, where σ_y is the yield stress.

The initial lateral crookedness for each specimen is carefully measured after setting the model arch on the test frame. The distance between the string stretched from a springing to another springing and the vertical string hung from the arch rib is carefully read with the aid of a 0.01 mm microscope. The maximum value and the shape of initial lateral crookedness are summarized in Table 5. Some of them exceed the tolerance $l/1000$ for initial crookedness of centrally loaded column specified in the Japanese Specification for Highway Bridges[14].

(5) Application of Load

The uniformly distributed load is idealized by groups of eight concentrated loads as shown in Figs. 6 or 7. The beams installed in the loading apparatus are connected mutually with hinges so as to be free for rotation about both in-plane and out-of-plane directions. The longitudinally unsymmetric load (Case V_2) can be applied by shifting the hydraulic jack adequately in the longitudinal direction, and the transversely unsymmetric load (Case V_1) can be applied by using some attachments. Since the model arch is supposed to be of through type, the lateral displacement of the loading beam is restrained,

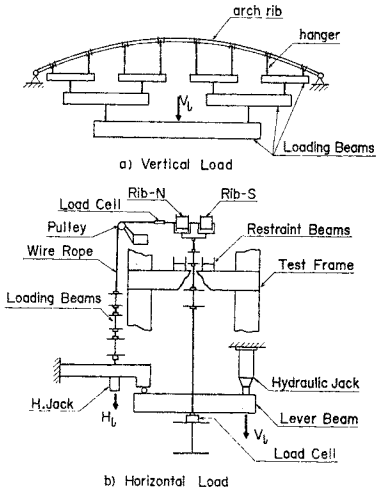

Fig. 6 Loading Apparatus.

Fig. 7 General View of the Loading Apparatus.

Fig. 8 Restraint of Loading Beams.

as shown in Fig. 8, in such a way that the actual hanger load can be simulated. The magnitude of the individual concentrated load is checked by wire strain gages bonded on the individual hanger. The measured load distribution is enough uniform except in the high loading stage near the ultimate state, in which the effect of the large deflection of the model arch appear.

(6) Measurement of Strain and Displacement

Twelve wire strain gages are bonded for each section of which measured values are desired. The distribution of the plastic zone illustrated later is obtained by judging the part plastic according to the fact that the sum of the residual strain due to welding and the additional strain produced by the applied load exceeds the yield strain. In order to know the magnitude and the mode of lateral deflection and rotational angle of cross section, a pair of electrical displacement meters is attached 20 cm apart from each other to an arm fixed to the arch rib as shown in Fig. 9. The measurement is done at seven points which divide the arch span into eight equal parts.

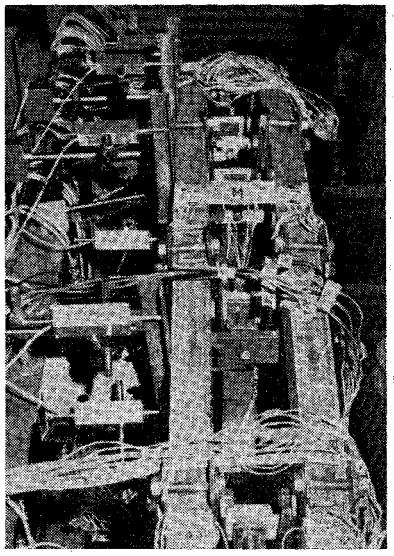

Fig. 9 Measurement of Lateral Displacements.

(7) Test Procedure

In the cases of vertical loading, the vertical load, V_l, is increased step by step until the test specimen becomes unstable. In the cases of horizontal loading, the horizontal load, H_l, applied in the direction from rib-S to rib-N, is increased step by step until the test specimen collapses, accompanying unbounded lateral displacement. In the latter case, the vertical load, V_l, which may correspond to vertical dead and live loads of actual bridges, is kept constant.

In what follows, the total vertical load, V_e, and the total horizontal load, H_e, are defined by the sums of the applied load, V_l or H_l, and the dead

load of the loading beam, V_a or H_a, respectively.

3. DISCUSSION OF TEST RESULTS

(1) Theoretical Estimation of the Ultimate Strength of the Model Arch

The ultimate strength and the inelastic spatial behavior of the model arch are analyzed by the matrix stiffness method considering the elasto-plastic large deflections. The detailed description of the theory is available in Ref. 8). The computation techniques adopted for the analysis of these model arches are as follows:

1) Since the theory is based on the finite element method, each arch rib is divided longitudinally into 16 member elements, and each bracing member is treated as one element.
2) In order to trace the growth of the plastic zone, the cross section of the arch rib is also divided into 28 segments. The modified value of the residual stress shown in Fig. 5 is given in each segment as an initial stress.
3) The initial Z-coordinate of each nodal point is presumed to be equal to the measured value of the initial lateral crookedness at the point.
4) The vertical type and the horizontal type of loads idealized in 15 and 17 nodal forces, respectively. The former nodal forces considered in the computation are applied in the direction of gravity or of the inclined hanger as shown in Fig. 10.

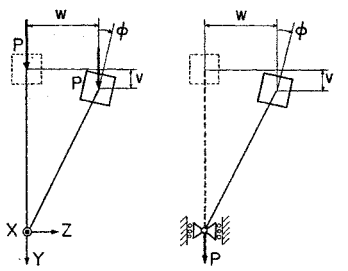

i) Gravity type load ii) Hanger load

Fig. 10 Load Direction in Theoretical Analysis.

5) The horizontal type of load is increased after the specific vertical load was applied. The loading sequence is non-proportional and this is the same condition in the test.
6) Theoretical maximum load is defined as the average of the critical load in equilibrium and the subsequent load at which any corresponding displacement can be no longer found in the incremental approach.

(2) Ultimate Strength

The experimental maximum loads of the model arches are summarized in Table 6 in comparison with the theoretical ones. Though the ultimate strength of the specimen may be affected by the residual stress, initial lateral crookedness, the type of the bracing member, the arch configuration and so on, the theoretical prediction shows fairly good correspondence with the experimental result except the specimen No. 12, which collapsed owing to the local failure of the arch rib near the springing. The validity of the theoretical study may be recognized. The collapse mode of the specimen No. 3 was difficult to distinguish, but it was classified into in-plane instability, because the in-plane sway displacement was rather dominant in comparison with the lateral displacement. Several specimens after test are shown in Fig. 11. Since various factors together with test techniques show combined effects on the ultimate strength of the model arch, the individual effect of the each factor could not be studied separately in the test. But, effects of the several factors are discussed qualitatively in what follows.

Table 6 Comparison of Maximum Loads.

a) Vertical Loading

Test No.	Collapse Mode	Test V_e ton	Theory V_t ton	V_e/V_t ×100%	Max. Values of Initial Lateral Crookedness
1(C-S-V)	Out-of-Plan	24.97	22.8	110	l/1 480
2(C-3P-V)		55.72	47.5	117	l/1 230N, l/1 480S
3(C-3L-V)	In-Plane	52.22	48.5	108	l/550N, l/940S
4(P-S-V)	Out-of-Plane	25.72	25.0	103	l/1 140
5(P-3P-V)		53.72	48.5	111	l/690N, l/760S
6(P-3L-V)		56.22	64.8	87	l/1 120N, l/1 520S
7(P-7P-V_1)		49.72	50.9	98	l/1 010N, l/1 320S
8(P-7X-V_1)		45.82	47.4	98	l/190N, l/300S
9(P-S-V_2)	In-Plane	18.52	17.9	104	l/1 270

b) Horizontal Loading

Test No.	Collapse Mode	Test V_e ton	Test H_e kg	Theory V_t ton	Theory H_t kg	H_e/H_t ×100 %	Remarks
10 (P-7P-H)	Out-of-Plane	40	3 705	40	3 325	111	
11 (P-7L-H)		50	3 705	50	3 780	98	
12 (P-7X-H)		50	2 305*	50	5 240	44*	*Local failure of the arch rib

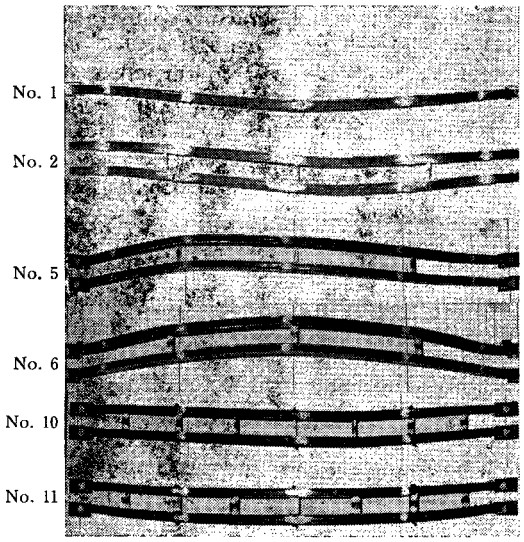

Fig. 11 Specimens after Test.

(3) Effects of Arch Configuration

The difference of the arch configuration, i. e., circular or parabolic, will make a much difference in the shape of the in-plane bending moment diagrams as shown in Fig. 12, where M_p denotes the full plastic moment. The effect of the difference in the in-plane bending moment can be also seen in the distribution of plastic zone as shown in Figs. 13 and 14. The plastic zone due to in-plane bending moment is developed in the upper flange near the crown of the circular arch (Fig. 13), but not in the parabolic arch (Fig. 14) except the plastic zone due to lateral bending. But, the final effect of the arch configuration on the ultimate strength may not be appreciable in both experimental and theoretical results of the specimen No. 1 through No. 6. This fact has

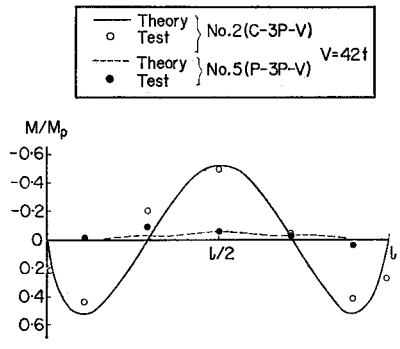

Fig. 12 Variation of In-plane Bending Moment.

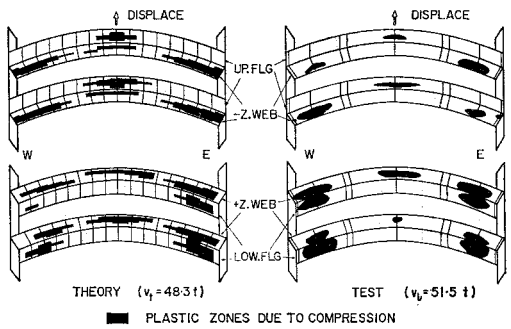

Fig. 13 Distribution of the Plastic Zone at the Ultimate State (No. 3).

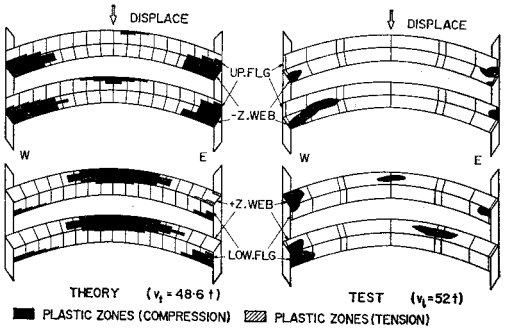

Fig. 14 Distribution of the Plastic Zone at the Ultimate State (No. 5).

been also shown in the general parametric study for the arch whose rise to span ratios are from 0.1 to 0.2[4].

(4) Effects of Bracing Members

Effects of the bracing system can be seen in the lateral bending moment diagrams of the arch ribs as shown in Fig. 15 for the model arch subjected to the horizontal type of load. The diagram shows discontinuity of the bending moment at the nodal points where the transverse beams are located. The extent of the discontinuity depends upon the rigidity of the transverse beam. It is apparently seen that the difference of the type of transverse beams makes the difference in the shape of the diagram. Since the transverse beam of type-P has comparatively small resistance, the shape of the bending moment diagram for the specimen No. 10 is similar to that of a single arch or a clamped-clamped beam. On the other hand, for the specimen No. 11 with beams of type-L, the magnitude of the lateral bending moment both at the crown and the springings is fairly

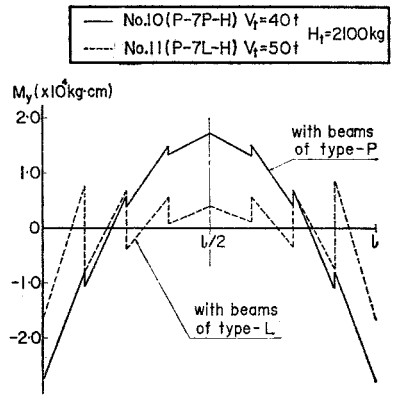

Fig. 15 Lateral Bending Moment Diagram (Theory).

Table 7 Decomposition of Lateral Bending Moments at the Springings (Theory).

Test Specimens	Bending Moment ($\times 10^4$ kg·cm) M_d	M_{s1}	M_{s2}	M_t	$M_d/M_t \times 100$ (%)
10(P-7P-H)	0·62	0·61	0·62	1·85	34
11(P-7L-H)	1·14	0·37	0·34	1·85	62
12(P-7X-H)	1·11	0·30	0·25	1·66	67
Remarks	V_t=10ton, H_t=500kg				

$M_t = M_d + M_s = M_d + M_{s1} + M_{s2}$

M_d: bending moment of twin ribs

M_s: bending moment of individual rib

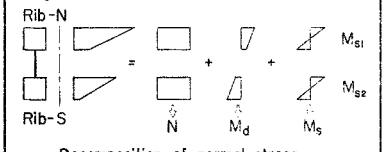

Decomposition of normal stress

reduced. Accordingly, the transverse beam of type-L is effective to decrease the lateral bending moment of the arch rib. This fact can be also recognized from the theoretical result for the model arch subjected to the vertical type of load.

The effect of the bracing system may be also known from the extent of the cooperative moment resistance in the braced twin ribs. The total lateral bending moment at the springings of the braced twin arches may be decomposed into two parts of lateral bending moment as illustrated in the inset of Table 7. The integral bending moment of twin ribs, M_d, and the sum of the bending moment in the individual rib, M_s, for the specimens No. 10, 11 and 12 are shown in Table 7 together with the ratios of M_d to the total bending moment, M_t. The larger the ratio is, the more effective bracing system can be obtained. It will be recognized again that the type-X, type-L and type-P are effective, in this order, to achieve the integral beam action of the braced twin ribs. These facts also mean that the bracing system of type-L or type-X is effective to increase the lateral bending stiffness of the whole structures.

The effect of the bracing system on the ultimate strength can be seen by comparing the specimens No. 7 and No. 8 with the specimen No. 4. Eccentrically loaded ribs of the specimens No. 7 and No. 8 can carry more than 120% of the ultimate load of the single rib arch, No. 4. But, the difference in the ultimate strength between various type of the bracing system could not be made clear for the case of vertical loading because of the influence of other factors. On the other hand, for the cases of horizontal loading, the specimens No. 10 and No. 11 are identical in the ultimate strength, though the vertical load of the specimen No. 11 is larger than that of the specimen No. 10. This fact corresponds to the above-mentioned conclusion drawn from the theoretical result.

In the previously published paper[5] of the writers, it was pointed out that the bracing member of type-X, which will play rather the same role as the transverse beam of type-L, may have a possibility to fail owing to a premature buckling. Since these models were not planned to observe such a phenomenon, the

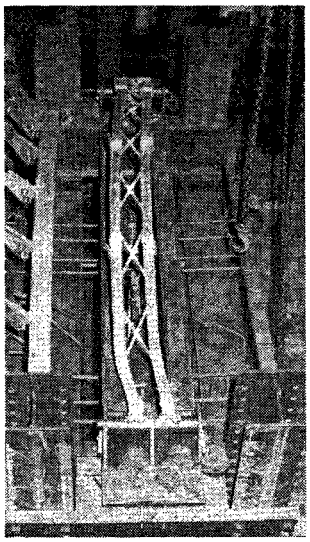

Fig. 16 Local Failure of the Arch Rib near the Springing in Specimen No. 12.

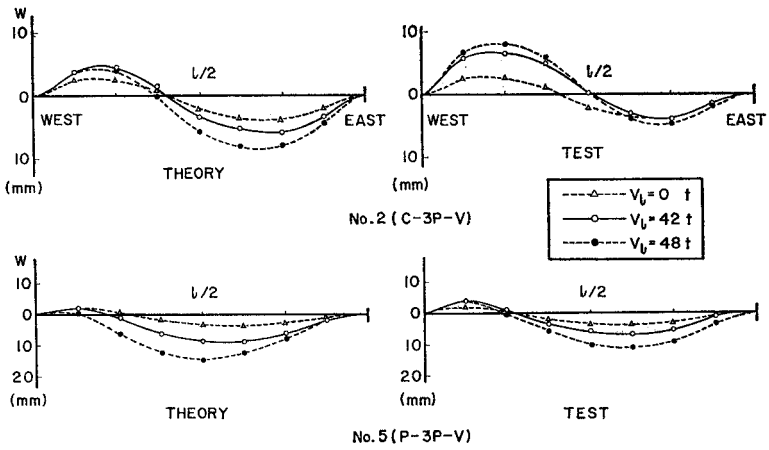

Fig. 17 Modes of Lateral Deflections.

premature buckling of the bracing member did not appear in the test. But, it was recognized experimentally that as for the specimen No. 12, whose bracing members were designed to be sufficiently stiff so as not to fail owing to the premature buckling, a local failure of the arch rib occurs at the part near the springing as shown in Fig. 16. This fact suggests the necessity of giving the adequate stiffness to the lateral member of truss type in order to ensure the enough strength of twin arches as a whole.

(5) Effects of Initial Lateral Crookedness

Some typical lateral deflection modes are shown in Fig. 17. It is notable that the shape of the initial lateral crookedness, in general, has an important effect upon the shape of lateral deflection mode under the vertical type of load. In the theoretical result, the larger wave between two initial waves of different sign grows more rapidly than the smaller one, and then the mode of lateral deflection show a tendency to become one wave. This tendency was not necessarily observed in the test because of the difficulty to realize the expected loading condition perfectly. Effects of the initial lateral crookedness on the ultimate strength may be controlled, in general, by its maximum value rather than its shape.[9] This fact may be recognized from the comparison of the maximum loads between the specimens No. 7 and No. 8, which are subjected to the same condition. The maximum load of the specimen No. 8 with large initial deflection is smaller than that of the specimen No. 7, though the specimen No. 8 has more effective lateral bracing system than that of the specimen No. 7.

The torsional angle of the arch rib was also measured, but was not shown here because of its small magnitude. But, it is useful to point out that the deformation mode of the arch rib subjected to the vertical type of load can be regarded as a lateral flexural buckling mode rather than a flexural-torsional buckling mode as shown in Fig. 11. This is because of the fact that the model arch composed of closed cross section has fairly stiff torsional rigidity of $GI_x/EI_y=0.5$. The torsional angle of the whole cross section will arise from the difference of in-plane deflections between both ribs.

(6) Effects of Residual Stress

The magnitude of the compressive residual stress and their pattern are very important because the premature yielding caused by them will reduce the stiffness of the arch ribs considerably[4),6)]. The appreciable effect of the residual stress pattern can be recognized from the fact that the premature yielding initiates at the central part of the component plate and spreads transversely as shown in Figs. 13 and 14. The effect of the residual stress pattern may be also recognized from the fact that the plastic zone due to tension appears in the arch springings of the specimen subjected to the horizontal load as shown in Fig. 18. In this connection, the shear stress due to torsion was not considered in this experimental determination of the plastic zone, because the measured values of the torsional angle and the shear strain due to torsion were fairly small for these model arches with closed cross section.

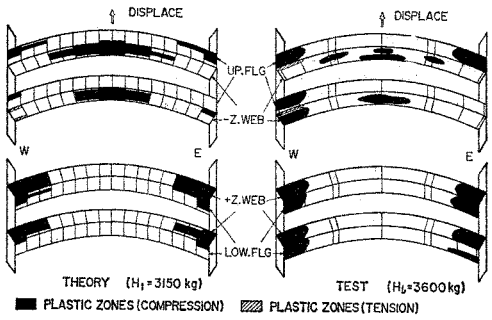

Fig. 18 Distribution of the Plastic Zone at the Ultimate State (No. 10).

For the specimens No. 10 and 11 which are subjected to the horizontal load after the preloading of the specific vertical load, the strain reversal, i.e., the unloading was observed at the springings. But, it seems that the local strain reversal in such cases may not have so important effects on the ultimate strength of the arch as a whole.

Furthermore, it is notable that all of the specimens tested herein become unstable before so-called plastic hinge appears, even in the cases of horizontal loading. Accordingly, it may be recognized that the structure like the arch, which is composed of compressive main members, should be analyzed under consideration of the longitudinal spread of the plastic zone.

(7) Effects of Load Directions

Table 8 shows the difference of the theoretical values of the maximum loads between the cases of the gravity-type load and those of the hanger load. Since the lateral restraint of the loading beam was not perfect in the test, the experimental values drop between these two sorts of theoretical predictions. For the cases of vertical loading, the theoretical predictions of the gravity-type load give adequate and safe side values. But, for the horizontal loading cases, the theoretical predictions of the gravity-type load seem to give too conservative values.

Table 8 Maximum Loads for Different Load Direction in Theory.

a) Vertical Loading

Test Specimens	Test V_e (ton)	Theory V_t (ton)	V_e/V_t (%)	Remarks
2 (C-3P-V)	55.72	47.5 (G) 49.8 (H)	117 112	G: Gravity type load H: Hanger load (see Fig. 10)
3 (C-3L-V)	52.22	48.5 (G) 48.8 (H)	108 107	
4 (P-S-V)	25.72	25.0 (G) 35.9 (H)	103 72	
5 (P-3P-V)	53.72	48.5 (G) 64.2 (H)	111 84	
6 (P-3L-V)	56.22	64.8 (G) 73.5 (H)	87 77	

b) Horizontal Loading

Test Specimens	Test H_e (kg)	Theory H_t (kg)	H_e/H_t (%)	Remarks
10 (P-7P-H)	3 705	1 800 (G) 3 325 (H)	206 111	*Local failure of the arch rib
12 (P-7X-H)	2 305*	2 070 (G) 5 240 (H)	111 44*	

ACKNOWLEDGMENTS

This experimental study was carried out at the Kumamoto University in four years from 1974 to 1977. The writers are indebted to Dr. Itio Hirai of Kumamoto University for his valuable encouragement. The writers wish to express their gratitude to Messrs. H. Ando, M. Aoki, K. Yamauchi, H. Yamashita, H. Enomoto and M. Kitano for their valuable assistance shown in the tests. Part of this study was supported by the Funds of Aid from the Ogawa Scholarship Association and by the Funds of Aid for Scientific Researches from the Ministry of Education. The numerical computations were carried out by the FACOM 230–75 computer of Kyushu University.

REFERENCES

1) Johnston, B. G.: Guide to Stability Design Criteria for Metal Structures, 3rd Ed. John Willey & Sons, New York, pp. 476–487, 1976.
2) Column Research Committee of Japan: Handbook of Structural Stability, Corona Publishing Co. Ltd., Tokyo, 1971.
3) Kee, C. F.: Lateral inelastic buckling of tied arches, Jour. of ST. Div., Proc. of ASCE, Vol. 87, No. ST1, pp. 23–39, Jan., 1961.
4) Sakimoto, T. and S. Komatsu: Ultimate load carrying capacity of steel arches with initial imperfections, Preliminary Report of Second International Colloquim on Stability of Steel Structures, held at Liege, Belguim, pp. 545–550, April, 1977.
5) Sakimoto, T. and S. Komatsu: A possibility of total breakdown of bridge arches due to buckling of lateral bracings, prepared discussion presented at the Second International Colloquim on Stability of Steel

Structures, held at Liege, Belgium, April, 1977, Final Report pp. 299–301, Oct., 1977.
6) Komatsu, S. and T. Sakimoto: Ultimate load carrying capacity of steel arches, Jour. of ST. Div., Proc. of ASCE, Vol. 103, No. ST12, pp. 2323–2336, Dec., 1977.
7) Komatsu, S., T. Sakimoto and K. Kobayashi: An experimental study on the ultimate strength of monochord Lohse girder, Kyoryo, June, 1976. (in Japanese)
8) Komatsu, S. and T. Sakimoto: Nonlinear analysis of spatial frames consisting of members with closed cross-section, Proc. of JSCE, No. 252, pp. 143–157, Aug., 1976.
9) Schulz, G.: Die Traglastberechnung von planmässig mittig belasteten Druckstäben aus Baustahl unter Berücksichtigung von geometrishen und strukturellen Imperfectionen, Dissetation eingereicht an der Technishen Hochschule in Graz, Juni, 1968.
10) Öustlund, L.: Lateral stability of bridge arches braced with transverse bars, Transactions of the Royal Institute of Technology, Stockholm, Sweden, No. 84, 1954.
11) Kuranishi, S.: The torsional buckling strength of solid rib arch bridge, Transactions of JSCE, No. 75, pp. 59–67, July, 1961. (in Japanese)
12) Tokarz, F. J.: Experimental study of lateral buckling of arches, Jour. of ST. Div., Proc. of ASCE, Vol. 97, No. ST2, pp. 545–559, Feb., 1971.
13) Sakimoto, T. and Y. Namita: Out-of-plane buckling of solid rib arches braced with transverse bars, Proc. of JSCE, No. 191, pp. 109–116, July, 1971.
14) Japan Road Association: Specification for Highway Bridges, Feb., 1973.

(Received May 20, 1978)